Computers and Concrete, Vol. 5, No. 5 (2008) 435-448
DOI: http://dx.doi.org/10.12989/cac.2008.5.5.435

Numerical modeling of drying shrinkage behavior of self-compacting concrete

How-Ji Chen† and Te-Hung Liu‡

Department of Civil Engineering, National Chung-Hsing University, Taichung 402, Taiwan

Chao-Wei Tang‡†

Department of Civil Engineering & Engineering Informatics, Cheng-Shiu University, Koahsiung 833, Taiwan

(Received January 30, 2007, Accepted September 17, 2008)

Abstract. Self-compacting concrete (SCC), characterized by the high flowability and resistance to segregation, is due to the high amount of paste (including cement and mineral admixtures) in contrast with normal concrete (NC). However, the high amount of paste will limit the volume fractions of coarse aggregate, and reduce the tendency of coarse aggregate to suppress drying shrinkage deformations. For this reason, SCC tends to produce higher values of drying shrinkage than NC for the most part. In order to assess the drying shrinkage of SCC quantitatively for application to offshore caisson foundations, the formulas presented in the literatures (ACI 209 and CEB-FIP) are used to predict the values of drying shrinkage in SCC according to the corresponding mix proportions. Additionally, a finite element (FE) model, which assumes concrete to be a homogeneous and isotropic material and follows the actual size and environmental conditions of the caisson, is utilized to simulate stress distribution situations and deformations in the SCC caisson resulting from the drying shrinkage. The probability of cracking and the behavior of drying shrinkage of the SCC caisson are drawn from the analytic results calculated by the FE model proposed in this paper.

Keywords: self-compacting concrete; drying shrinkage; caisson foundation.

1. Introduction

Drying shrinkage is the volume change of hardened concrete mainly caused by the loss of water from the cement gel. Drying shrinkage also depends on numerous factors, such as the properties of cement paste, the content of aggregate, mix proportions, size and shape of structure, curing, and environmental conditions (temperature and relative humidity), etc. Moreover, the reduction of volume in concrete due to drying shrinkage could deform the structure. Because the deformations in the structure are restricted by the constraints of geometric boundary conditions and affected by variations in shrinkages, which probably results in stress redistribution in the structure and tensile stresses in the concrete. Once the tensile stresses formed by drying shrinkage exceed the tensile strength of concrete itself, the concrete would develop cracks simultaneously and become deficient

† Professor, Corresponding Author, E-mail: hjchen@mail.ce.nchu.edu.tw
‡ Postgraduate, E-mail: d9262101@mail.nchu.edu.tw
‡† Associate Professor, E-mail: tangcw@csu.edu.tw

in its service. For mass concrete, cracks may likely be found on the surface of a structure especially in the first few days after casting (Mehta and Monteiro 2005). The drying shrinkage of mass concrete is mainly caused by the uneven distribution of humidity, which also leads to different shrinkage strains in corresponding sections (Mindess, *et al*. 2003, Kim and Lee 1998).

As regards an offshore mass concrete caisson foundation, the densely arranged reinforcing bars make NC difficult to be placed, and the severe requirements of durability and water tightness of concretes due to the offshore environment make the use of NC inappropriate. In contrast, the use of SCC leads to lots of advantages. The superior characteristics of workability and resisting segregation provide convenience to construction, eliminate some of the potential problems for human error that generally caused by the improper placing or vibration, and limit the occurrence of honeycombs in the structure. SCC will not only reduce the technical costs of in-situ cast concrete construction, but also improve the quality, durability and reliability of the concrete structure (Okamura and Ozawa 1995). According to the above-mentioned, SCC is more suitable for offshore caisson foundations than NC.

However, when using SCC, this type of concrete needs a more advanced mix design than traditional vibrated concrete (Su, *et al.* 2001, Brouwers and Radix 2005). The most crucial reason is the high amount of paste used in SCC. This results in higher values of drying shrinkage and lower values of elastic modulus than NC (Persson 2001, Domone 2006(a), 2007(b)) because of the relatively lower amount of aggregate providing restraint in concrete. In particular, the effects on volume stability of the concrete should be paid more attention to in structural analysis (Chen, *et al.* 2004). As for caisson structures, the excessively high surface to volume ratio (s/v) may bring about larger drying shrinkage. In practice, the critical regions in the caisson structure with the most likelihood of cracking are conventionally inspected by a nondestructive test (NDT) based on the Time-of-Flight Diffraction Technique (Lin and Su 1996, Lin, *et al.* 1999). Because the geometry and large dimensions of the caisson structure, the measurement would be difficult. By contrast, the effective selection and diminution of the test locations become significant (Bonda, *et al.* 2000).

For above reasons, a FE model is proposed based on the real scale of the offshore caisson structure to conduct analysis by the commercially available program. The drying shrinkage strain in different sections of mass concrete structures was evaluated in accordance with various prediction equations (ACI 209 1992, CEB-FIP 1991). The calculated drying shrinkage strain is then transformed into an equivalent stress according to a general Hook's law, which is then applied to the FE model. The strains corresponding to equivalent stress were used to simulate the drying shrinkage strain.

2. Reliability of numerical calculation

The precision of numerical calculation depends on whether the result is convergent after calculation. Different mesh methods were used to test the precision of the numerical calculation. The actual dimensions of the caisson, a rectangular block (18 m in height and 16 m in width) with 16 rectangular hollow parts are shown in Fig. 1(a). The thickness of internal and external walls is 25 cm and 60 cm respectively. Considering the symmetric deformations of the actual caisson resulting from drying shrinkage, the numerical model is regarded as a 1/8 caisson (as shown in Fig. 1(b)). The geometric symmetry of the structure is significant and essential for FE analyses because the mesh of symmetric partition can reduce the number of elements drastically and improve the efficiency simultaneously with the same precision as that of an entire structure. As a result, the boundary condition of the numerical model is treated so that the bottom is only constrained in the Z

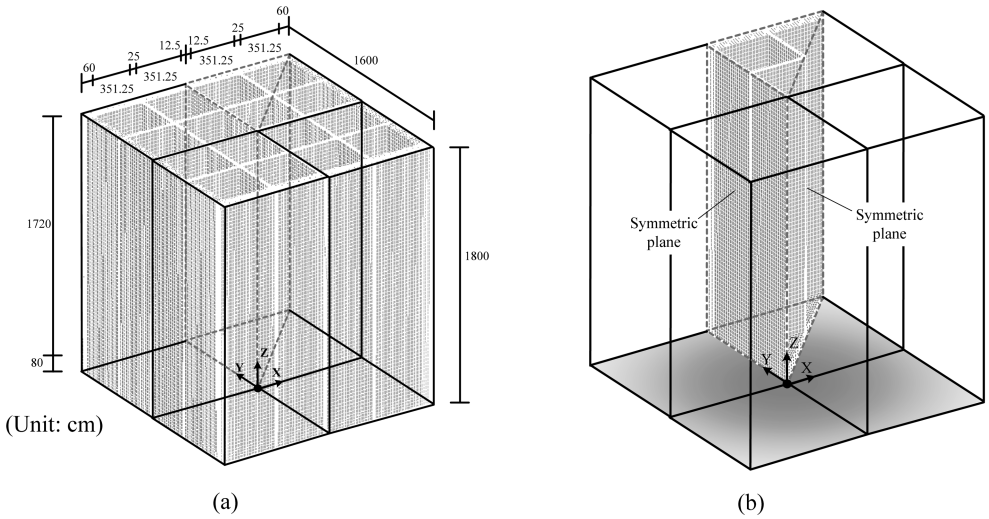

Fig. 1(a) Dimensions of the caisson, (b) Numerical model of 1/8 caisson

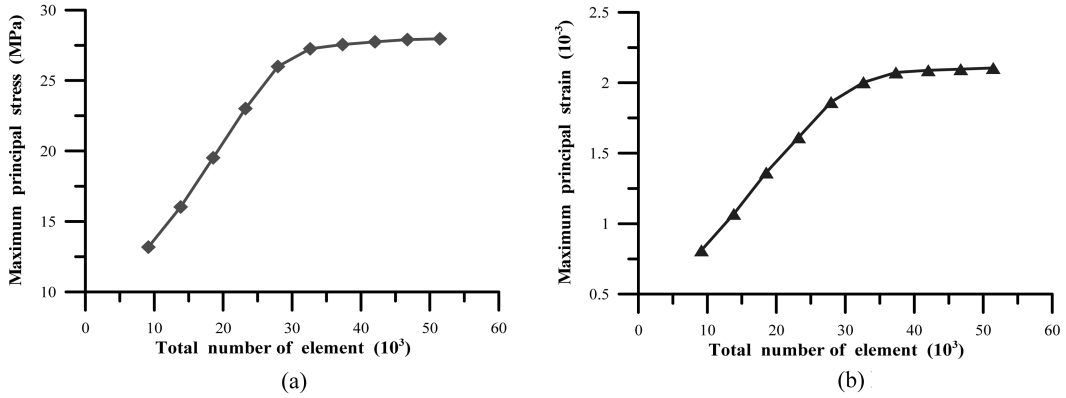

Fig. 2 Maximum principal stresses of the caisson

direction and the symmetric plane is only constrained in the normal direction. That is to say, the center of the bottom is fixed in the three directions (X-, Y-, and Z-axis) and which is also a center of symmetry when the caisson contracts. Besides, the aspect ratio of element is kept under 4 and the inside angle at each corner is between 45° to 135°. A uniform distributed stress P applied from inside radiates toward the outside to simulate a container enduring an internal exploding stress. An internal pressure of 5 MPa is applied. The material parameters include compressive strength (f_c') = 38 MPa, E = 15.3 GPa and ν = 0.2. The result of the numerical calculation (Fig. 2) shows that if more than 30,000 elements are used, both principal stress and strain converge. If it is greater than 35,000, no matter what meshing methods are chosen, the result is almost the same. The maximum deviation of the principal stress or principal strain is within ±0.5%. That means the proposed mesh method is very precise. Therefore, a total element number over 35,000 is adopted for the following analysis.

3. Prediction of drying shrinkage

There are many empirical equations that have been developed for the prediction of shrinkage. The most common approaches are those of ACI and CEB. The empirical equations recommend by ACI 209 (1992), CEB-FIP (1991) and J.K. Kim (1998) were adopted to predict the shrinkage strain inside mass concrete.

3.1. ACI 209R-92 Method

ACI Committee 209 recommended this empirical equation in 1992 that allows shrinkage to be estimated as a function of time of drying and ultimate shrinkage. The shrinkage, $(\varepsilon_{sh})_t$, at any time t after an age of 7 days for moist cured concrete is given by

$$(\varepsilon_{sh})_t = \frac{t}{35+t}(\varepsilon_{sh})_u \tag{1}$$

where $(\varepsilon_{sh})_u$ is the value of ultimate shrinkage. The effect of others properties of concrete are given by correction factors:

$$(\varepsilon_{sh})_u = 780 \cdot \gamma_{cp} \cdot \gamma_\lambda \cdot \gamma_h(\gamma_{vs}) \cdot \gamma_s \cdot \gamma_\varphi \cdot \gamma_c \cdot \gamma_\alpha \times 10^{-6} \tag{2}$$

where

- γ_{cp}:

Initial moist curing days	1	3	7	14	28	90
γ_{cp}	1.2	1.1	1.0	0.93	0.86	0.75

- γ_λ:

$$\gamma_\lambda = \begin{cases} 1.40 - 0.01\lambda\ , & \text{for} \quad 40 \le \lambda \le 80 \\ 3.00 - 0.030\lambda, & \text{for} \quad 80 > \lambda > 100 \end{cases}$$

λ : relative humidity (%)

- γ_{vs}:

$\gamma_{vs} = 1.2\exp(-0.00472v/s)$
v/s : volume to surface ratio

- γ_s :

$\gamma_s = 0.89 + 0.00161s$
s : slump (mm)

- γ_φ :

$$\gamma_\varphi = \begin{cases} 0.3 + 0.0024\varphi, & \text{for} \quad \varphi \le 50\% \\ 0.90 + 0.002\varphi, & \text{for} \quad \varphi > 50\% \end{cases}$$

φ : fine aggregate percentage (%)

- γ_c :
  $\gamma_c = 0.75 + 0.00061\,c$
  c : cement content (kg)
- γ_α :
  $\gamma_\alpha = 0.95 + 0.008\,\alpha$
  α : air content (%)

3.2. CEB-FIP 1990 Method

CEB-FIP 1978 prediction formula of drying shrinkage was later corrected in 1990 to be CEB-FIP 1990. The traditional CEB-FIP 1978 tends to neglect some material parameters; hence, its predictions are relatively weak. The corrected CEB-FIP 1990, however, considered the material parameters of 28-day compressive strength and types of cement. The detailed prediction formula is as follows:

$$\varepsilon_{cs} = \varepsilon_{cso} \cdot \beta_s(t - t_s) \tag{3}$$

where ε_{cs} is the shrinkage strain at time t after drying commences at time t_s; ε_{cso} is the basic shrinkage coefficient, which depends on relative humidity, type of cement and compressive strength of concrete. ε_{cso} is given by

$$\varepsilon_{cso} = \varepsilon_s(f_{cm}) \cdot \beta_{RH} \tag{4}$$

where:

$$\varepsilon_s(f_{cm}) = \left[160 + 10\beta_{cs}\left(9 - \frac{f_{cm}}{f_{cmo}}\right)\right] \cdot 10^{-6}$$

f_{cm} = compressive strength (MPa)
f_{cmo} = 10 MPa
β_{sc} = 4, low heat cement
5, normal cement
8, high early strength cement

$$\beta_{RH} = \begin{cases} -1.55 \cdot \beta_{sRH}, & 40\% \le RH \le 99\% \\ +0.25 \quad\quad , & RH \ge 99\% \end{cases}$$

$$\beta_{sRH} = 1 - \left(\frac{RH}{RH_0}\right)^3$$

RH = relative humidity (%)
RH_0 = 100%

β_s is a function corresponding to the change of shrinkage with time, which depends on specimen dimensions, is given by

$$\beta_s(t - t_s) = \left[\frac{(t - t_s)/t_1}{350(h/h_0)^2 + (t - t_s)/t_1}\right]^{0.5} \tag{5}$$

where

h = $2A_c/u$ (mm)
A_c = cross section (mm^2)
u = perimeter (mm)
t_1 = 1 day
h_0 = 100 mm

3.3. Kim and Lee method

The prediction equation proposed by J.K. Kim and C.S. Lee allows shrinkage to be estimated as a function of time of drying and length of the diffusion path. The shrinkage, $\varepsilon(y, t)$, is given by

$$\varepsilon(y,t) = ae^{b\lambda} \tag{6}$$

where
a: 353×10^{-6} for w/c 0.65
238×10^{-6} for w/c 0.40
b: –415.4 for w/c 0.65
–426.1 for w/c 0.40
λ:$y/\sqrt{t}$
y: length of the diffusion path (m)
t : shrinkage hours

All data (Table 1) needed for the prediction formula are based on the design information of the

Table 1 Data used in prediction formulas

f'_c (MPa)	Slump (mm)	Water (kg/m^3)	Cement (kg/m^3)	Aggregate (kg/m^3)	
				Fine	Coarse
38	270	194	308	833	797
Air content (%)		R.H. (%)	Type of cement		
1		65	Type I–Portland cement		

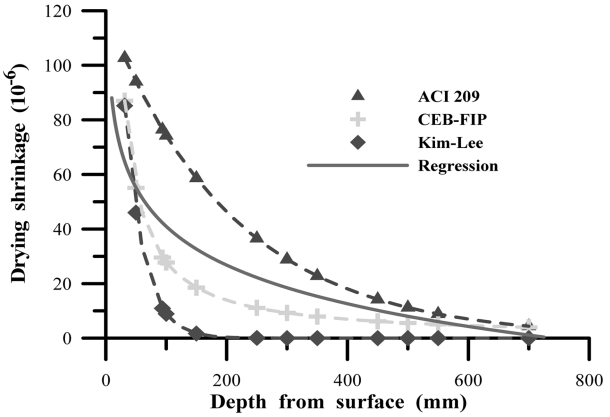

Fig. 3 Predictions and regression shrinkage strain at 7 days of age

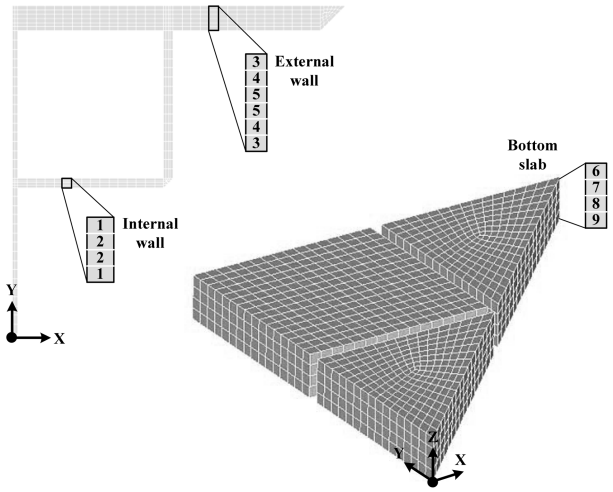

Fig. 4 Arrangement of elements

Table 2 Equivalent stresses at each element

		Internal wall		External wall			Bottom slab			
Serial number of element		1	2	3	4	5	6	7	8	9
Regressed	Shrinkage strain (10^{-6})	65	42	55	33	22	41	18	8	1
$\begin{pmatrix} ACI-209 \\ CEB-FIP \\ Kim-Lee \end{pmatrix}$	Equivalent stress (MPa)	1.61	1.05	1.37	0.81	0.55	1.02	0.46	0.20	0.01

caisson. For comparisons, the predictions are carried out up to 7 days, which is the duration before the caisson is placed into water. The results of the predictions are shown in Fig. 3. It can be seen that the predictions of the shrinkage strains according to the CEB and Kim-Lee formulas are very closer and, however, the result according to the ACI prediction formula is significantly different. To obtain a neutral prediction, the average drying shrinkage strain can be obtained by averaging out the results of the three prediction formulas. From the results of Fig. 3, the drying shrinkage strain on any section in the container can be obtained. The value is then transformed to equivalent stress for the numerical calculation. The respective equivalent stress is shown in Table 2 while the corresponding element position and serial numbers are shown in Fig. 4.

4. Concept of equivalent stress

Since the value of concrete strain cannot be considered as an input, the drying shrinkage strain is transformed into an equivalent stress by numerical calculations. It is assumed that the materials are homogeneous and elastic; the relationship between the drying shrinkage strain and the equivalent stress can be derived according to general Hook's law.

The stress-strain formula of general Hook's law is

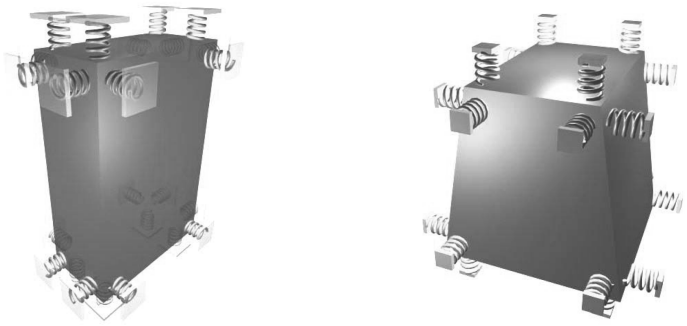

(a) (b)

Fig. 5 3-D solid element

$$\varepsilon_x + \varepsilon_y + \varepsilon_z = \frac{1-2\nu}{E}(\sigma_x + \sigma_y + \sigma_z) \tag{7}$$

where ν is Poisson's ratio, E is elastic modulus, ε and σ represent respectively the strain and stress; the subscripts denote the directions of the Cartesian axes.

Assuming that the element would shrink homogeneously, the strains and stresses in the three axes are isotropic. Therefore, one has

$$\sigma = \frac{E}{1-2\nu}\varepsilon \tag{8}$$

where ε and σ represent respectively the drying shrinkage strain and equivalent stress.

Two 3-D solid elements with different shapes were chosen for verifying the applicability of the concept of equivalent stress. By using an element (Solid Brick 8 nodes 45 element) with an aspect ratio of 2:1:3 (length: width: height), a linear spring (Beam 4 element) is added at each node in three directions with stiffness approaching zero (See Fig. 5(a)). The material parameters were used according to the actual concrete data, which are E = 21.3 GPa, ν = 0.2, and the drying shrinkage strain was assumed 800μ. The equivalent stress calculated by the conversion formula Eq. (8) is 28.4 MPa. Tri-axial uniform stress placed onto the element (shown in Fig. 5) for calculation. The results of drying shrinkage strains in the X-, Y-, and Z-axis directions are all 800μ, the same as the assumed value. Another analysis performed used a tapered element as shown in Fig. 5(b). All parameters used are the same as the element described above. After calculation, the drying shrinkage strains in the X-, Y-, and Z-axis directions can be determined are 800μ, respectively. The strain result of the finite element analysis shows that the concept of equivalent stress is feasible.

However, the corresponding stress result is not the real stress caused by shrinkage. The original equivalent stress must be subtracted from the result after analysis. In order to verify the point, a beam frame is analyzed. Suppose that each element of this beam endures 800μ shrinkage strain in the Z-axis direction (as shown in Fig. 6(a)). By the assumption of linear-elastic material, the original beam can be regarded as the combination of two structures – Fig. 6(b) and Fig. 6(c) according to the superposition principle. Fig. 6(b) represents each element subjected to the fixed-end stresses with equal value but opposite direction of equivalent stresses. There are no relative deformations between elements in this case. Fig. 6(c) is the original beam applying the equivalent stresses. It possesses real shrinkage deformations without any modification. However, the real stresses resulting

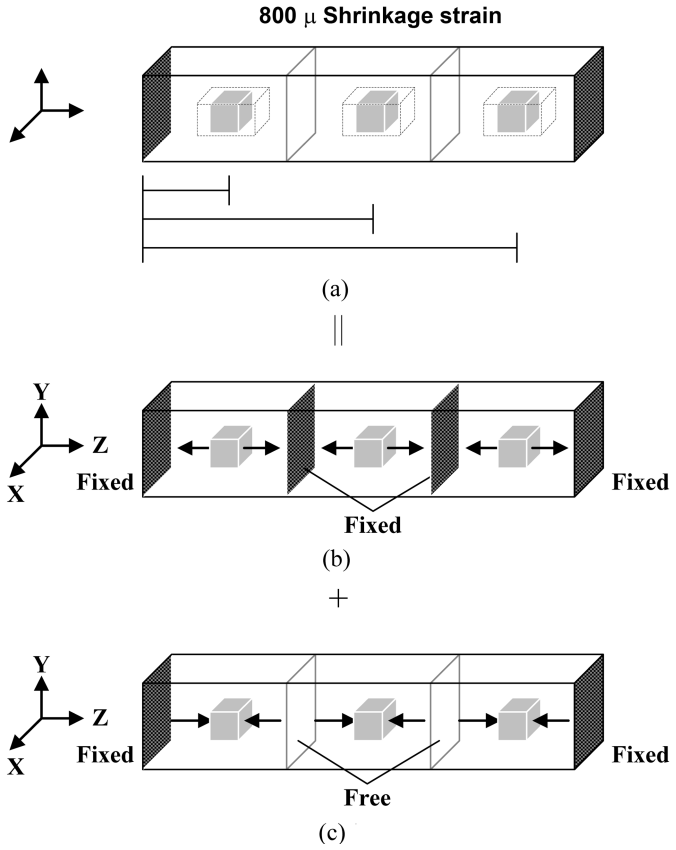

Fig. 6 (a) *Original beam* with 800 μ shrinkage strain, (b) *Fixed-end stresses* (= – equivalent stresses), (c) *Equivalent stresses* applied on original beam without initial shrinkage

Table 3 Comparison of theoretical and numerical solutions

	Beam	L/4	L/2	3L/4
$\sigma_{z\ (MPa)}$	Numerical solution	17.06	17.06	17.06
	Theoretical solution	17.06	17.06	17.06
ε_z	Numerical solution	1.17E-18	-1.17E-19	-1.17E-18
	Theoretical solution	0	0	0

from shrinkage (Fig. 6(a)) must be obtained by subtracting equivalent stresses from the stresses in Fig. 6(c). The comparison of theoretical and numerical solutions at three different places in this beam is listed in Table 3. Due to the boundary condition of the two fixed ends, the theoretical solution is zero and the numerical solution of strain in the Z-axis direction approaches zero. As to stress, after subtracting equivalent stress from the numerical solution, the solution is the same as the theoretical one (shown in Table 3). The result verified the applicability of the concept of equivalent stress.

In addition, because the realistic shrinkage is not the same in every part of a mass concrete structure, three prediction formulas, the specification of ACI 209 (1992), CEB-FIP (1991) and the

formula proposed by J.K. Kim and C.S. Lee (1998), were used to determine the amount of drying shrinkage strain. Stress and strain caused by shrinkage can be obtained according to the equivalent stress concept.

5. Numerical analysis

5.1. Deformation of the caisson

The drying shrinkage strains, regressed from the results of the three prediction formulas (see Fig. 3), were used to predict the drying shrinkage behavior of the caisson. The shape of the caisson model suffering from drying shrinkage deformation is shown in Fig. 7. The displacement of nodes ranges from 0.11~0.38 mm in the X- and Y-axis direction, and 0.68~0.89 mm in the Z-axis direction. The figure shows that the bottom slab provides resistance to restrain the caisson from deforming in the X- and Y-axis direction. Therefore, the transverse deformation of the caisson increases with height and the maximum occurs in the top layer. However, the influence of the bottom slab on the vertical deformation of the caisson is comparatively insignificant, and primarily depends on the axial stiffness of walls in the Z-axis direction. Obviously, the external wall possesses higher stiffness than the internal wall, and therefore brings about the lower corresponding values of displacement deservedly.

As mentioned above, the constraints contributed from the bottom slab and the external wall will cause larger variations of deformation in the internal wall, which is one of the major causes that may result in tensile stresses in concrete due to shrinkage. It can be initially expected that the maximum shrinkage stresses will be found in the regions of the internal wall close to the bottom slab and the external wall in terms of the feature of deformation of the caisson model.

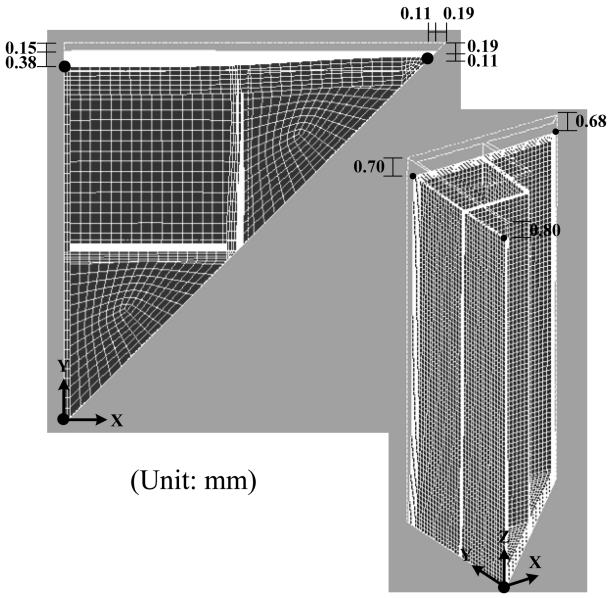

Fig. 7 Deformation of the caisson

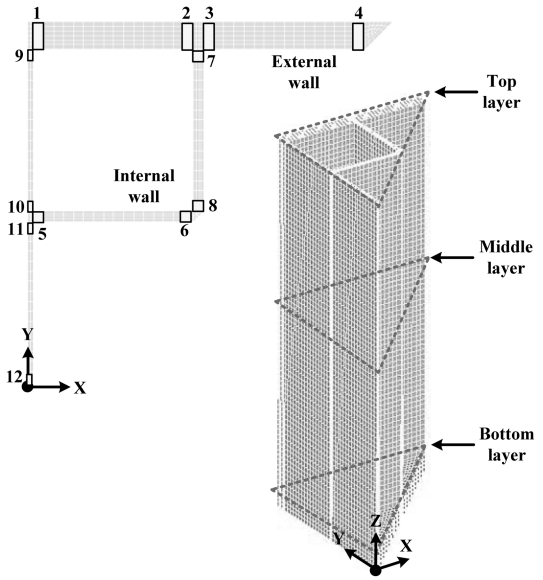

Fig. 8 Regions selected for the stress output

5.2. Shrinkage stresses in the caisson

Since the real stress caused by shrinkage must be obtained by subtracting the original equivalent stress from the results of numerical analysis, the procedure could be considerably complicated and time-consuming for taking all the elements into account. For this reason, certain critical regions drawn from deformation of the caisson model that likely cause larger shrinkage stresses are selected for output (see Fig. 8).

The maximum principal stresses of the numerical calculation from the top layer, the middle layer and the bottom layer of the numerical model of caisson (see Fig. 1(b)) for critical regions are shown in Fig. 9. The principal stress lies between 0~0.72 MPa in the external wall (Fig. 9(a)) as well as –0.03~0.94 MPa in the internal wall (Fig. 9(b)). The positive and negative values represent tensile and compressive stresses, respectively. For the stress distribution in concrete, the tensile stresses distributed on the interior sections of concrete are relatively mild, and there is a steep rise in the area near the surface. This phenomenon is in accordance with the theoretical predictions (Fig. 3) and which is primarily related to the gradient of the regression curve. In the surface area, the variation of shrinkage is extreme, but rapidly tends to be steady and close to be zero with the increase of distance from surface. Moreover, the tensile stress increases sequentially from the top to the bottom layer, as it is influenced by the constraint of the bottom slab.

As to the comparison of the external and internal wall, the larger and even the maximum tensile stress (region 9) is found in the surface area of the bottom of the internal wall. The result is consistent with the theoretical predictions. The external wall plays a role of contributing more

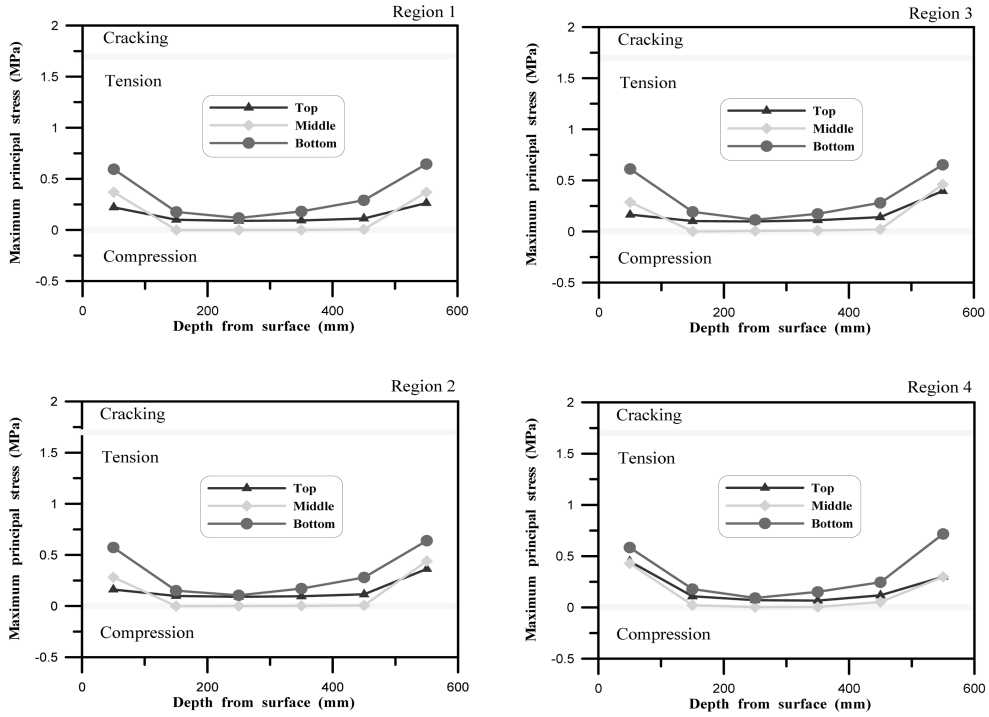

Fig. 9(a) Distributions of principal stresses in the external wall

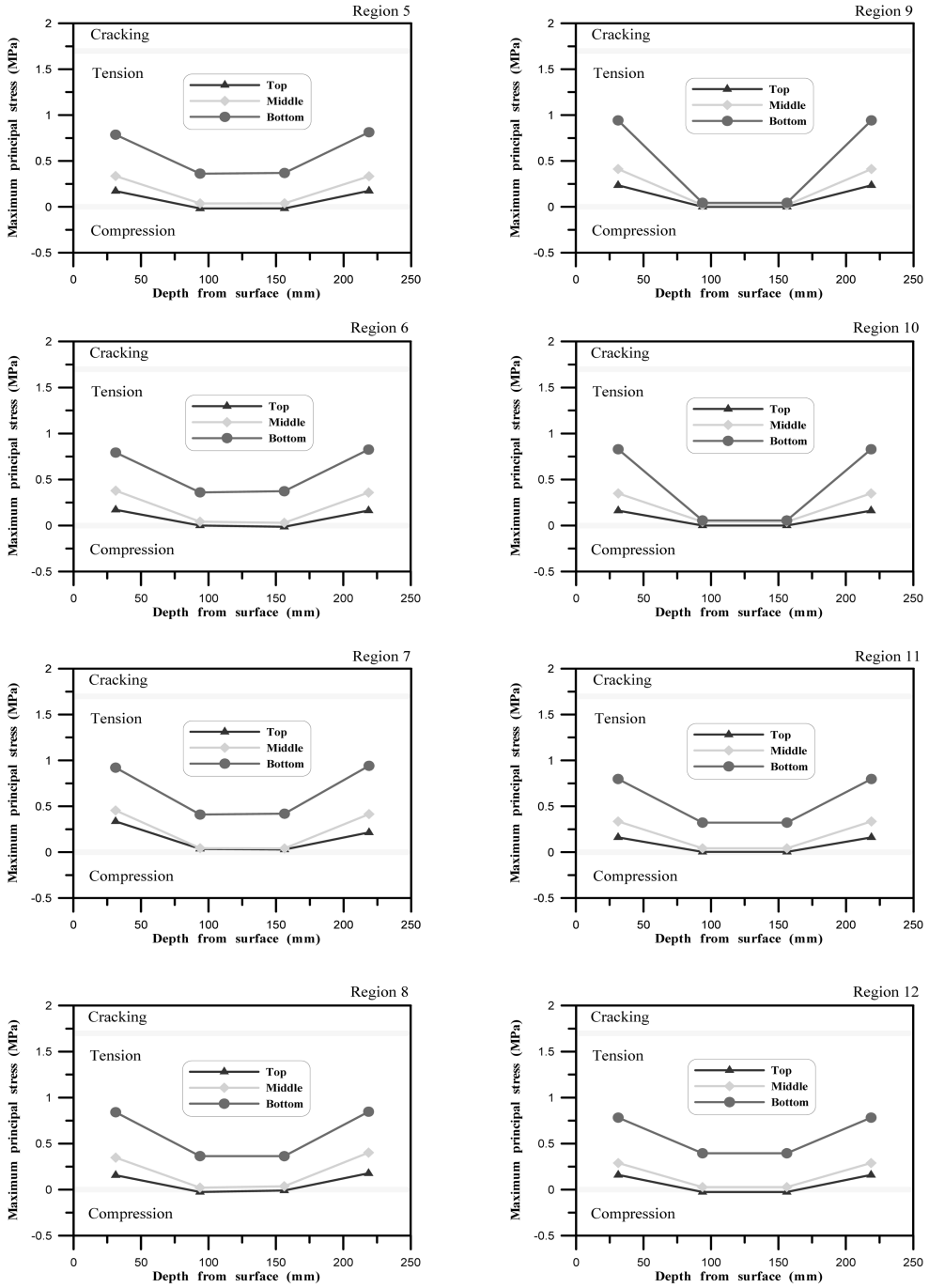

Fig. 9(b) Distributions of principal stresses in the internal wall

constraints than the internal wall does. The deformation of the internal wall near to the external wall will change with an intense variation, and the variation of deformation will also produce the additional increment of tensile stresses in concrete.

Tensile strength is an important property of concrete that greatly affects the extent and the size of cracking in structures. Literature (Mehta and Monteiro 2005, Mindess, *et al.* 2003) indicates that the tensile/compressive strength ratio depends on the level of compressive strength. In general, the ratio of tensile strength to compressive strength ranges from 0.07 to 0.14. In this study, a more conservative value of 7% of the compressive strength is used for SCC to predict stress that may cause cracking on the concrete. Furthermore, since the development of drying shrinkage will be stopped for concrete in water due to the full supply of moisture, the duration of drying shrinkage before the caisson placed into water (7 days) should be consider as shrinkage time. The compressive strength of SCC at 7 days is 24.3 MPa, and the corresponding tensile strength ranging from 1.7 MPa (7% of compressive strength) is used to simulate the actual situation of caisson. As shown in Fig. 9, the maximum tensile stress caused by shrinkage is 0.94 MPa (region 9), and which is under the values of tensile strength of SCC estimated at 7 days. This indicates that, for the case of this study, SCC is able to attain the requirements for the application to offshore caisson foundations. The probability of shrinkage cracking in caisson foundations should be limited.

The numerical analysis model follows the actual caisson sited in Port of Taichung in Taiwan. Since the in-place nondestructive tests are not able to cover the entire caisson, it is important to provide sufficient test locations and reliable measurement characterizing the caisson adequately. The selected test locations to the caisson in the field include the corresponding critical regions of numerical model (Fig. 8). The in-place test results indicate that the developed cracks could be found more frequently in these critical regions. This cracking situation in the caisson was mitigated substantially after fortified by incremental reinforcing steels. Through the prior evaluation by numerical analysis, reinforcement may be provided for the critical regions of caisson with high risk of cracking before construction. The durability of caisson could also be improved consequently.

6. Conclusions

A numerical method proposed in this paper is used to simulate the behaviors of drying shrinkage and to predict the probability of cracking in a SCC caisson foundation. The conclusions can be summarized as follows:

1. The numerical calculation results show that a better convergence can be achieved if the total element number over 35,000. The aspect ratio (length, width and height) of the element is within 4 and the mesh angle of the element is between 45° and 135°. The maximum deviation of principal stress or principal strain is within ±0.5%.
2. Based on the deformation situations of the caisson, the larger deformation variation with higher tensile stress is found in the internal wall connected to the bottom slab and the external wall. The regions selected for calculating the real stresses from the FE model after analysis can also be reduced.
3. For the stress distribution in the caisson, the maximum tensile stress is 0.94 MPa (region 9) and which is under the values of tensile strength of SCC (1.7 MPa). This means SCC is able to attain the requirements for the application to offshore caisson foundations. The probability of shrinkage cracking should be limited.
4. For shrinkage cracking analysis of mass concrete structures (especially for the caisson structures with large dimensions), the numerical method of applying equivalent stresses in the FE model could speedily and precisely determine the critical regions throughout the structure, and provide useful alternatives and supplements for in-place tests to eliminate the unnecessary test locations.

References

ACI Committee 209 (1992), *ACI 209-92: Prediction of Creep, Shrinkage and Temperature Effects in Concrete Structure*, "American Concrete Institute", Farmington Hills, MI.

Bond, L.J., Kepler, W.F., and Frangopol, D.M. (2000), "Improved assessment of mass concrete dams using acoustic travel time tomography. part itheory", *Construction and Building Mater.*, **14**(3), 133-146.

Brouwers, H.J.H. and Radix, H.J. (2005), "Self-compacting concrete: theoretical and experimental study", *Cement and Concrete Res.*, **35**(11), 2116-2136.

CEB-FIP (1991), "CEB-FIP Model Code 1990 (Design Code)", Final Draft, Thomas Telford Ltd., London.

Chen, H.J., Peng, H.S., and Chen, Y.F. (2004), "Numerical analysis of shrinkage stresses in a mass concrete", *J. the Chinese Ins. Eng.*, **27**(3), 357-365.

Domone, P.L. (2006), "Self-compacting concrete: An analysis of 11 years of case studies", *Cement Concrete Compo*., **28**(2), 197-208.

Domone, P.L. (2007), "A review of the hardened mechanical properties of self-compacting concrete", *Cement Concrete Compo.,* **29**(1), 1-12.

Kim, J.K., and Lee, C.S. (1998), "Prediction of differential drying shrinkage in concrete", *Cement and Concrete Res.*, **28**(7), 985-994.

Lin, Y., and Su, W.C. (1996), "Use of stress waves for determining the depth of surface-opening cracks in concrete structures", *ACI Mater. J.*, **93**(5), 494-505.

Lin, Y., Liou, T., and Tsai, W.H. (1999), "Determining the crack depth and the measurement errors using time-of-flight diffraction techniques", *ACI Mater. J.*, **96**(2), 190-195.

Mehta, P.K. and Monteiro, P.J.M. (2005), *Concrete: Structure, Properties, and Materials*, Prentice-Hall, Englewood Cliffs, N.J.

Mindess, S., and Young, J.F., and Darwin, D., (2003), *Concrete*, Prentice-Hall, Englewood Cliffs, N.J.

Okamura, H. and Ozawa, K. (1995), "Mix-design for self-compacting concrete", *Concrete Library of JSCE*, **25**, 107-120.

Persson, B. (2001), "A comparison between mechanical properties of self-compacting concrete and the corresponding properties of normal concrete", *Cement Concrete Res.*, **31**(2), 193-198.

Sua, N., Hsu, K.C., and Chai, H.W. (2001), "A simple mix design method for self-compacting concrete", *Cement Concrete Res.*, **31**(12), 1799-1807.

CC